SPRINGER LINK

Log in

☰ Menu　　|　　🔍 Search　　　　　　　　🛒 Cart

Nanostructured Ce/CeO$_2$–rGO: Highly Sensitive and Selective Electrochemical Hydrogen Sulfide (H$_2$S) Sensor

Download PDF ⤓

Access provided by Dr. Babasaheb Ambedkar Marathwada University, Aurangabad
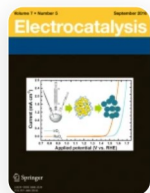
Electrocatalysis

Aims and scope

Submit manuscript

Shivsharan M. Mali, Shankar S. Narwade, Balaji B. Mulik, Vijay S. Sapner, Shubham J. Annadate & Bhaskar R. Sathe ✉

👁 235 Accesses　　Explore all metrics →

Abstract

Herein, cerium/cerium oxide nanoparticles have been decorated on reduced graphene oxide (Ce/CeO$_2$–rGO) for room temperature electrochemical determination of H$_2$S in 0.5 M KOH. There is a superior linear correlation between the peak current density and H$_2$S content in the tested range of 1–5 ppm. Moreover, comparison to other abundant gases such as CO$_2$ shows no

response at the potential of H_2S oxidation, confirming no interference with H_2S detection. It also reveals that the Ce/CeO$_2$-rGO nanocomposite is a highly selective and sensitive system for the determination of H_2S gas. Ce/CeO$_2$-rGO synthesized by a simple chemical approach and further characterized by X-ray diffraction (XRD), Fourier transform infrared (FTIR), field emission-scanning electron microscopy (FE-SEM), coupled energy dispersive analysis of X-ray (EDAX), and BET-surface area measurement confirms the porosity of synthesized nanomaterials and homogeneous decoration of Ce/CeO$_2$ nanoparticles on rGO sheets. The electrochemical studies, i.e., linear sweep voltammetry (LSV), of Ce/CeO$_2$-rGO demonstrate the electrochemical H_2S sensing at room temperature and for lower gas concentration (1 ppm) detection. The sensing mechanism is believed to be based on the modulation of the current and applied potential path across the electron exchange between the cerium oxide and rGO sites when exposed to H_2S.

Graphical Abstract

One-pot synthesis of Ce/CeO$_2$-GO hybrid nanostructure is of immense significance for H_2S gas sensors. Here is a new superficial synthetic way intended for the synthesis of Ce/CeO$_2$-GO nanocomposites through the sol−gel technique. Herein, we depict that the consequential Ce/CeO$_2$ NPs decorated on graphene oxide sheet material can give competent electrocatalysts for the H_2S oxidation reaction in an alkaline condition. The current density of 5.9 mA/cm^2 on the tiny potential of 2.5 mV vs. SCE demonstrates huge catalytic bustle and stability.
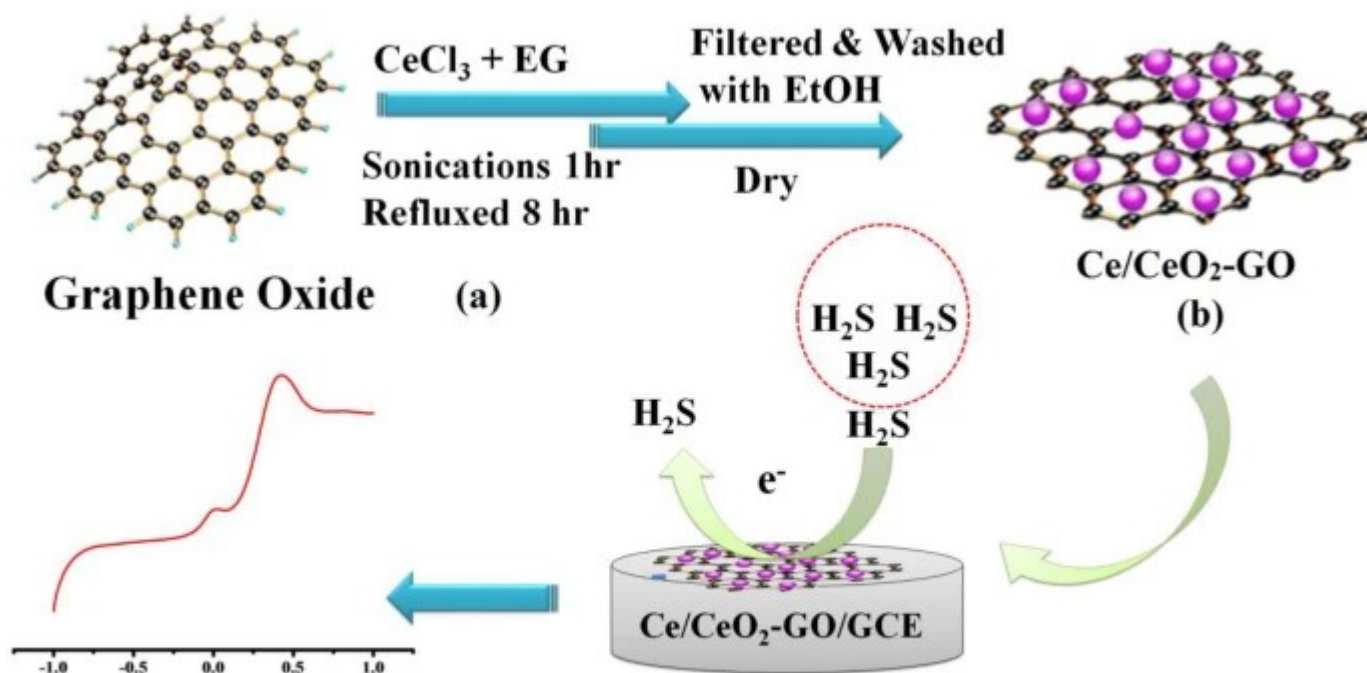
E(V) vs. SCE

**Electrochemical H₂S (d)
oxidation**

**Electrochemical H₂S (c)
sensing**

Similar content being viewed by others

MXene Key Composites: A New Arena for Gas Sensors

Article | Open access
06 June 2024
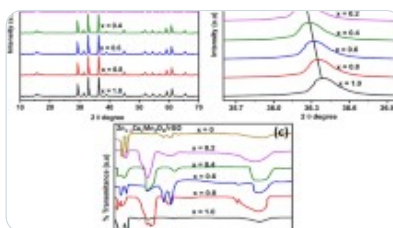
Effect of Copper Substitution on the Electrocatalytic Activity of ZnMn2O4 Spinel...

Article | 07 February 2023
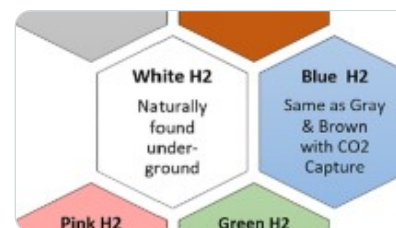
Platinum–Graphene Heterogeneous Catalysts for Hydrogen Mitigation Applications

Article | 12 June 2024

Use our pre-submission checklist →

Avoid common mistakes on your manuscript.

Introduction

Society is exposed to various air toxins in the indoor and outdoor environments. Poor air quality is a well-known cause for various health issues which can over and over again result into life-intimidating and sudden emergency care. H_2S is one of the common toxic air pollutants, which is mostly found as a mixture with other gases and at a very low concentration. It can direct to personal pain at a higher concentration, and it can result in loss of consciousness, lasting brain damage, or death due to the neurotoxicity produced by the gases [1]. H_2S releases through many industrial processes and it also produces by-products from many organic transformations and these gases are throughout the environment

(nature). For example, the primary sources of H_2S release includes by decomposition of organic materials by bacteria while it is also an ingredient of natural gases, volcanic gases, sulfur dump, and sulfur jumps [2]. The unmediated releases of high concentrations of sulfides can effectively overcome the checks and balances that job under natural situations and can significantly intimidate those close to the environment. Therefore, there is an increasing demand for highly sensitive, fast-responding, transportable devices for monitoring lower detection limits of sulfides in ecological and industrial areas. Hydrogen sulfide (H_2S) is a colorless, toxic, and flammable gas, with an odor unlike a rotten egg smell [3]. Instant leak H_2S gas to levels greater than 300 ppm is measured as hazardous to life or health [4]. Manufacturing processes relating to natural gas and oil, paper and pulp production, sewage treatment, and sulfur and its derivatives in manufacturing plants are lying onto potentially high levels of H_2S, that also go on naturally or as a side-product of the industrial processes [5]. Monitoring of both dissolved sulfide and H_2S is of great importance due to the high toxicity of sulfides which can cause stern or deadly poisoning due to the neurotoxic consequence of the gas [6]. Although dissolved sulfide has mobilized freely into aquatic (river, sea, and marine) environments and it is hazardous, the release of high concentrations of sulfide can be monitored and converted by electrochemical techniques [7].

Detection methods for sulfide have evolved from simple colorimetric assays to the more recently used techniques, including high-pressure liquid chromatography (HPLC) and gas chromatography (GC) [8,9,10], monobromobimane (MBB) [11,12,13,14], fluorescence probe [8], electrochemical sensors (ion-sensitive electrodes and polarographic H_2S sensors), high-performance fluorescence spectroscopy, iodometric titration, calorimetry, metal-induced sulfide precipitation, and conductivity/impedance methods based on metal-oxide (M-O) semiconductors [15,16,17,18,19,20,21,22]. On the other hand, large instrumentation, high costs, long preparation times and conditioning/processing of samples, and the need for standards and toxic chemicals, at least in some cases, make these analytical methods ineligible for their deployment in the field. Despite these drawbacks, electrochemical methods have gained immense popularity owing to massive development in instrumentation and techniques, lower cost, portability, simplicity of design, and rapid analysis with high selectivity and sensitivity [23,24,25,26,27]. In addition, the selection of sensing materials is also crucial to the sensing effect of the sensor [28]. In prior reports, H_2S sensors based on metal [29], carbon (C) [30, 31], and metal oxide (MO) [32,33,34] materials have been

developed and all these studies have achieved effectual results, though these materials have some insuperable shortcomings, such as low sensitivity, poor stability, and high cost [35, 36] which limit their application in electrochemical sensing. Herein, the detection of H_2S by the electrochemical method is suitable and easy having an exceptionally ultra-low detection limit (even can detect a single atom/molecule).

Different diagnostic methods have been reported and used for the detection of dissolved sulfides including spectroscopic, colorimetric, titrimetric, chromatographic, and electrochemical that give several ways such as in potentiometric and amperometric techniques [17, 18, 37,38,39]. Among these, electrochemical methods give a smart platform for industrial and ecological applications due to the ease of the move towards and the potential for online scrutinized systems. Electrochemical methods for H_2S were sensitive and selective to gas diffusion membrane. For example, Brown et al. examined the selectivity of several electro-polymerized membranes for selective H_2S determination against a wide range of interferences and found that phenylenediamine series performed better [37]. The Pt electrode has a huge cost that frequently reduces the sensor as sulfide ions to sulfur. Other materials enhance the overall H_2S sensing performance showing better LOD, selectivity vs. key interfering species, sensitivity retention in proteinaceous media, and response time. However, the more attractive potentiometric and amperometric systems have been used majorly for industrial H_2S sensing and monitoring purposes [40,41,42,43,44].

Ce/CeO$_2$–rGO nanostructures used for the construction of electrochemical sensors are vital to change the work conditions and develop the performance of as-prepared electrochemical sensors, such as sensitivity, working potential, selectivity, and linear range. The Ce/CeO$_2$–rGO nanostructures with a large specific surface area and multi-oxidation state Ce^{+3}, Ce^{+4} benign compatibility have provided a superior surface for adsorption of H_2S molecules at interface. Ce/CeO$_2$ is frequently used and plays an important role on the improvement of chemical gas sensing on graphene-based sensing systems [42,43,44]. As previously reported, Ce doping can increase the amount of the vacancy in host material via the transformation of chemical valence (Ce$^{4+}\rightarrow$ Ce^{3+}), which is very beneficial for enhancing the response to reducing gaseous species like H_2S [45, 46].

In this work, an electrochemical H_2S sensor integrates the H_2S oxidation reactions. It can be

converted into SO_2 through electrochemical reaction at Ce/CeO$_2$–rGO electrocatalytic interface. This proposed system theoretically provides an alternative street for the environmentally simultaneous monitoring of dissolved gases with additional fiscal and ecological benefits. Ce/CeO$_2$–rGO hybrid nanostructures exhibit excellent electrochemical performance, and these experimental results evidently expose the presence of the charge transfer (CT) at the edges of Ce/CeO$_2$ NPs and rGO, as schematically shown in Scheme 1.

Scheme 1
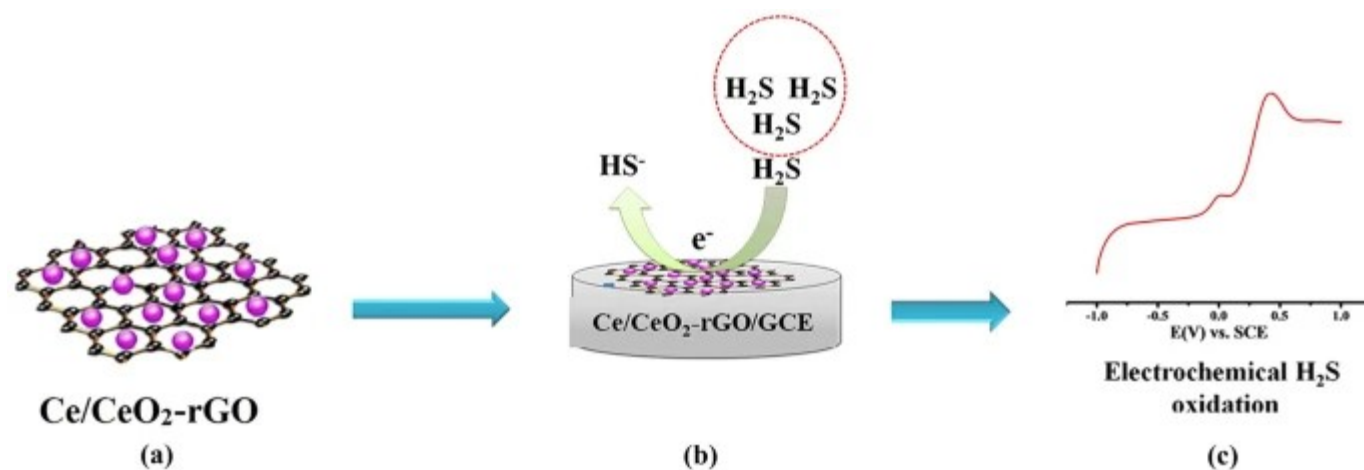
Schematic representation of a Ce/CeO$_2$ nanoparticles decoration on rGO surface, i.e., Ce/CeO$_2$–rGO, b exposure of H$_2$S gas towards Ce/CeO$_2$–rGO interface followed with electron transfer, and c corresponding to its oxidative determination by LSV performance studies

Experimental

Materials and Reagents

Sulfuric acid (H$_2$SO$_4$) 98%, nitric acid (HNO$_3$) 78%, and graphite powder 99.99% are of analytical grade. Cerium chloride (CeCl$_3$·7H$_2$O), hydrochloric acid, potassium hydroxide (KOH), H$_2$S gas cylinder, ethylene glycol (EG), absolute ethanol, and acetone were procured from SD Fine Chem, India. The whole organic solvents were retail of analytical rank and used with no additional decontamination. Deionized water (18 MΩ) from the Milli-Q system was used for all syntheses and electrochemical assessments of electrocatalytic materials.
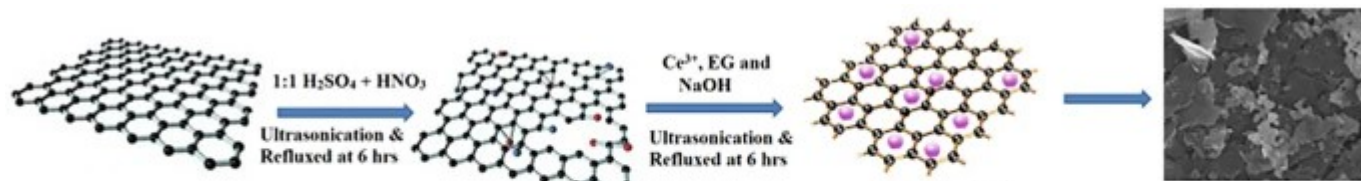
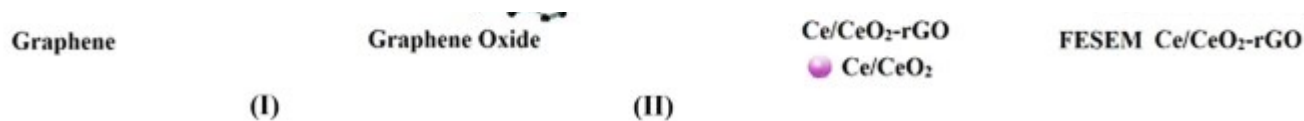# Chemical Synthesis of Graphene Oxide (GO) and Reduced Graphene Oxide (rGO)

The chemical synthesis acid-functionalized graphene oxide (GO) was synthesized initially. Eighty milligrams of graphite powder was taken in 100 mL mixture of 78% HNO_3 and 98% H_2SO_4 (1:1) and sonicated for a few minutes because the separate sheet of graphene creates suitable dispersion of graphene then refluxed for 6 h [45,46,47,48]. This leads to the carboxylation of graphene sheets from graphite followed by exfoliation into the solution, i.e., formation of GO. Then, the mixture was filtered by using polytetrafluoro ethylene (PTFE) membrane (pore size 0.2 µm) as well as the GO-based carbon mass was washed carefully with deionized water until the pH of the filtrate remains neutral (pH-7) followed with ethanol, then dried out at 60−80 °C in a furnace for 2 h. Furthermore, for the synthesis of rGO; 0.5 g of the above as-synthesized GO was taken and mixed with hydrazine hydrate (2−5 mL), and the mixture was stirred for 2 h. The dispersion was filtered, and the solid material was washed copiously with ethanol to remove excess hydrazine hydrate and other impurities. This as-synthesized rGO was further used for the synthesis of nanocomposite materials below.

Synthesis of Cerium−Cerium Oxide-Reduced Graphene Oxide (Ce/CeO$_2$−rGO) Hybrid Nanoelectrodes

For the synthesis of Ce/CeO$_2$−rGO hybrid electrocatalytic system, pre-synthesized 20 mg rGO was added into preheated 50 mL of anhydrous ethylene glycol (heated at 130 °C for 30 min to remove dissolved oxygen and water molecules) followed with ultra-sonication for 2 h to get fully exfoliated rGO sheets, and then added to it the calculated amount of 0.2 mg L^{-1} $CeCl_3 \cdot 7H_2O$ in the dispersion of rGO and ultra-sonicated further for 2 h. The suspension of Ce/CeO$_2$−rGO was mechanically stirred and refluxed for 6 h to form a Ce/CeO$_2$−rGO hybrid nanostructure. The substrate GO is converted to rGO, and could be due to oxygen containing all surface functionalities utilized for CeO$_2$ skin formation on Ce ions at rGO and Ce nanoparticle interface, i.e., Ce/CeO$_2$−rGO hybrid formation shown in Scheme 2.

Scheme 2

Graphene   Graphene Oxide   Ce/CeO₂-rGO   FESEM Ce/CeO₂-rGO
                                                                    Ce/CeO₂

(I)   **(II)**

Chemical synthesis method of (I) decoration of Ce/CeO$_2$ nanoparticles on rGO and (II) purification of Ce/CeO$_2$–rGO nanocomposites and FE-SEM

Instrumentation and Experimental Procedure

All electrochemical studies were performed on CHI-660E (CH-instruments USA) using a conventional three-electrode test cell with a Pt foil, and saturated calomel (SCE), glassy carbon (GC) electrode (3-mm dia.) were used as counter, reference, and working electrodes, respectively. Prior to the experiment, the cleaning of the working electrode was carried out by polishing it using three different (grain sizes 1.0, 0.3, and 0.05 μm) alumina powders, followed by washing with water (deionized water) and methanol (AR grade) to remove inorganic and organic impurities, respectively. All electrochemical/electroanalytical studies were carried out in an aqueous solution of 0.5 M KOH using a three-electrode system.

## Preparation of Modified Electrode for Electrochemical H2S Sensor

The modified Ce/CeO$_2$–rGO electrode was fabricated by the below procedure. During the first step, the bare glassy carbon (GC) electrode was instinctively refined with alumina powders of different sizes (0.3, 0.05, and 1.0 μm) on a micro-polishing kit and rinsed with methanol which was followed by ultrasonication to eradicate the alumina residues. In the second step, a 10 μL aliquot of Ce/CeO$_2$–rGO (2 mg in 0.18 mL of isopropanol and 20 μL of 5 wt% Nafion solutions) was drop-casted on the surface of cleaned GC surface and air-dried at room temperature [49].

Results and Discussion

Figure 1a shows a field emission–scanning electron microscopy (FE–SEM) image of rGO demonstrating the individual few layer sheets are $400-500$ nm in size. In Ce/CeO$_2$–rGO hybrid nanostructures as shown in Fig. 1b and c, Ce/CeO$_2$ NPs decorated entirely on the rGO framework like in this reference [45], which is able to attribute the better dispersion. The FE–SEM image of Ce/CeO$_2$–rGO hybrid nanostructures evidently shows the nanoparticles have a size of $50-100$ nm in this nanocomposite as shown in Fig. 1b. The formation of highly dispersed metallic Ce/CeO$_2$ NPs between narrow size distributions of $50-100$ nm observed on rGO support. As shown by FE–SEM in Fig. 1c, some particles are agglomerated [50].

Fig. 1
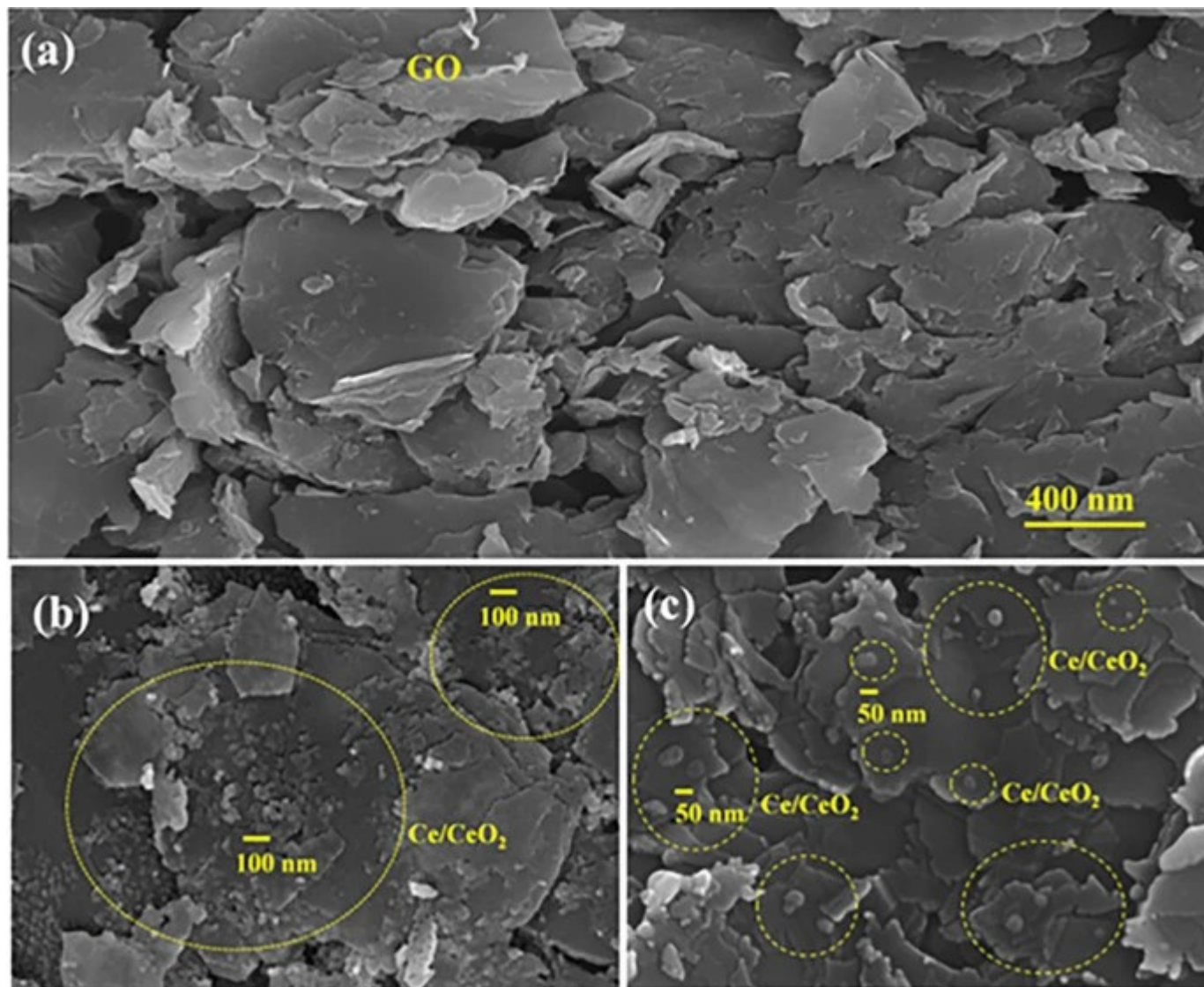
FE–SEM images of a GO and b, c of Ce/CeO$_2$–rGO hybrid nanostructures confirm Ce/CeO$_2$ embedded/ decorated on few layers of rGO and the size of Ce/CeO$_2$ NPs is in the range of 10−100 nm

The surface morphology of Ce/CeO$_2$–rGO is shown in Fig. 1b and c. The surface of rGO was covered by Ce/CeO$_2$ 50−100 nm in size of NPs and hierarchical interconnected nanoparticles of a porous network-like morphology are shown in Fig. 1b and c. These Ce/CeO$_2$ nanoparticles are vertically grown on sheets of graphene. Moreover, the SEM for bare Ce/CeO$_2$ has a homogeneous distribution of particles with a range of 10−100 nm as shown in Fig. 2.

Fig. 2
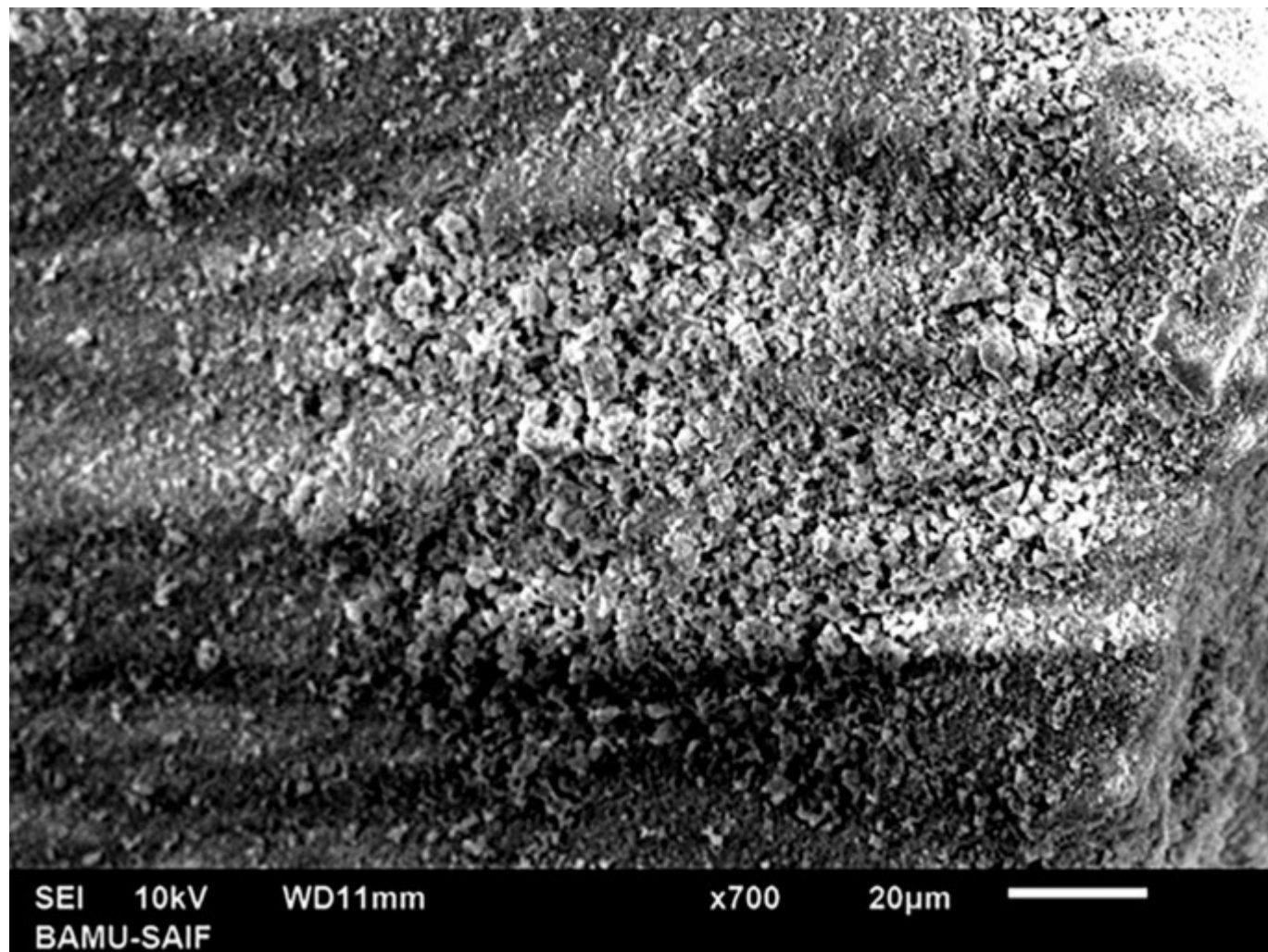
The FE-SEM image of bare Ce/CeO$_2$ has a homogeneous distribution of particles with a range of 10–100 nm

The elemental composition of the as-synthesized hybrid was analyzed using energy-dispersive analysis of X-ray (EDAX). Accordingly, Fig. 3 consisted of carbon (C), cerium (Ce), oxygen (O), sulfur (S), and nitrogen (N) with the wt% of 62.67, 14.47, 13.72, 7.54, and 1.59, respectively, conforming to the formation of Ce/CeO$_2$–rGO hybrid nanostructure and is in good agreement with XRD analysis as shown in Fig. 4. The presence of N, S, and O in the presence of C and Ce confirms the existence of defective sites through surface functionalities for anchoring Ce/CeO$_2$ NPs on rGO sheets. The presence of signals, their binding energy values, and representative wt% are in good agreement with the similar systems from literature [50].
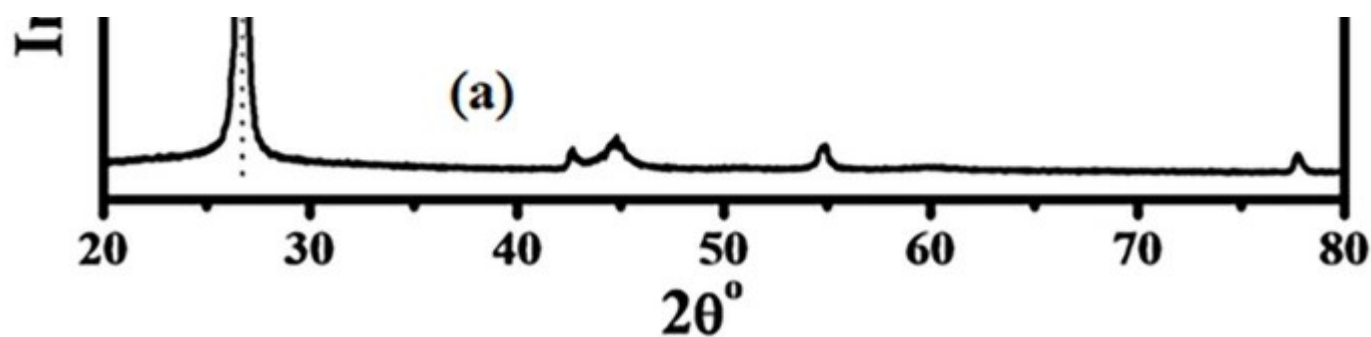
Fig. 3
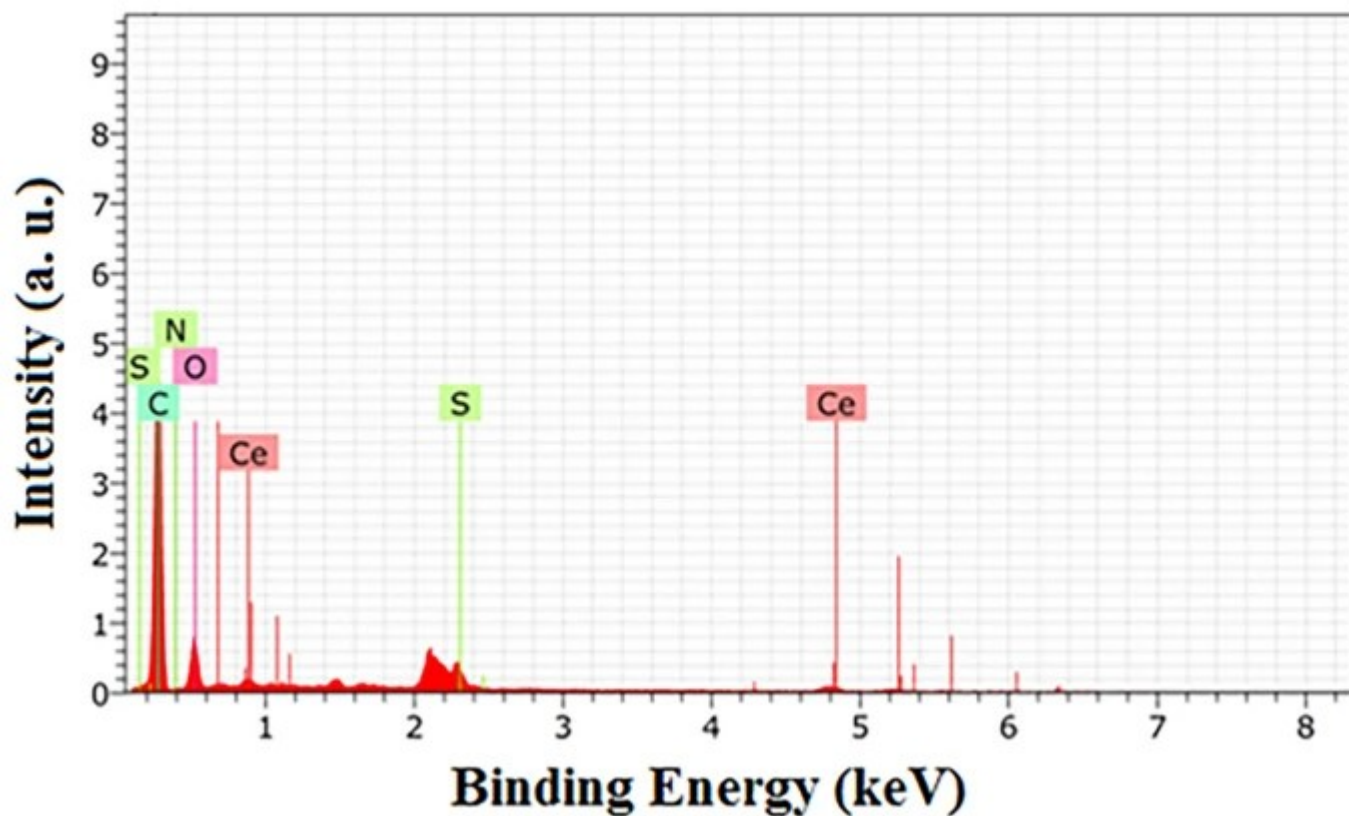
Energy-dispersive analysis of X-ray (EDAX) pattern of Ce/CeO$_2$-rGO corresponding to carbon (C), cerium (Ce), oxygen (O), sulfur (S), and nitrogen (N) with the wt% of 62.67%, 14.47%, 13.72%, 7.54%, and 1.59%, respectively

Fig. 4
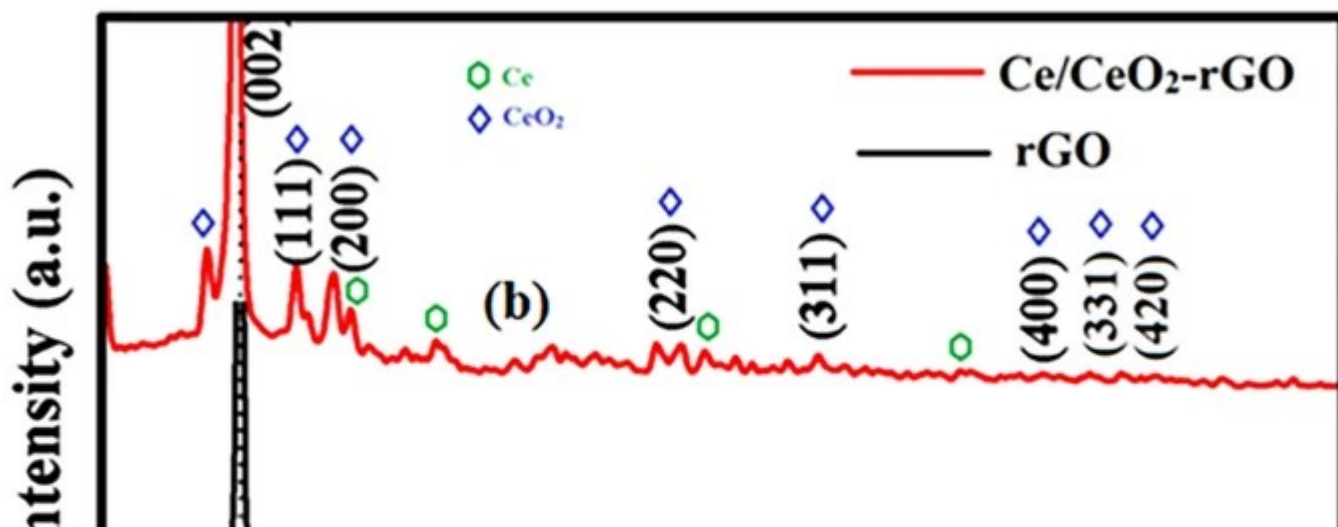
Superimposed X-ray diffraction (XRD) shows a rGO corresponding to few layers of graphene and b Ce/CeO$_2$-rGO hybrid nanostructure having mixed phases of rGO, and Ce/CeO$_2$ NPs, respectively

The superimposed X-ray diffraction (XRD) for the as-synthesized rGO and Ce/CeO$_2$-rGO hybrid nanostructures is shown in Fig. 4. Accordingly, the XRD pattern shown in Fig. 4a corresponds to a characteristic peak at $2\theta = 26°$ which can be assigned to (002) plane of rGO. Moreover, as shown in Fig. 4b, the corresponding planes (111), (002), (200), (220), (311), (400), (331), and (420) for Ce/CeO$_2$-rGO have crystalline lattice planes of CeO$_2$ and Ce of Ce/CeO$_2$ NPs on rGO. These peaks agreed well with the cubic structure of Ce/CeO$_2$. In the XRD pattern of Ce/CeO$_2$-rGO hybrid, both characteristic peaks for rGO and Ce/CeO$_2$ were observed, indicating that the as-prepared hybrid is composed of high-purity rGO and Ce/CeO$_2$ phases and is in good agreement with literature [51].

The as-synthesized hybrid Ce/CeO$_2$-rGO nanostructures were further characterized to confirm acid functionalization followed by its concern towards anchoring of Ce/CeO$_2$ NPs by using FTIR analysis shown in Fig. 5. In accordance with the literature, the acid treatment results into introduction of –OH, –COOH, –SO$_3$H, etc., functional groups on the rGO surface and these functionalities are responsible for further decoration of Ce/CeO$_2$ NPs on the surface. Consequently, the FTIR spectra confirm well-defined bands at C=C 1574 cm^{-1}, C=O 1655 cm^{-1}, –C-OH 1099 cm^{-1}, and Ce-O 603cm^{-1}, and remain near about corresponding band ranges of 1642−1829 cm^{-1}, 1516 cm^{-1}, and 1182 cm^{-1} which are characteristics of –C-H, –CO-OH, –C=C-, and –C-OH stretching frequencies corresponding to partial availability of oxidative functionalities on rGO. The band at 3355 cm^{-1} determines the –O-H containing groups as shown in Fig. 5a. Interestingly, after hybrid formation, an additional signal appeared at ~665−400 cm^{-1} corresponding to Ce-O along with the disappearance of bands corresponding to -O-

H, –COOH, and C–OH and the change in the frequencies of the representative bands supports the formation of Ce/CeO_2-rGO as shown in Fig. 5b. These results are also in good agreement with XRD, FE-SEM, and similar systems from literature [51]. Additionally, FTIR spectra of Ce/CeO_2 NPs obtained using KBr pellet methods are shown in SI (Fig. S1), with appropriate scientific discussions.

Fig. 5
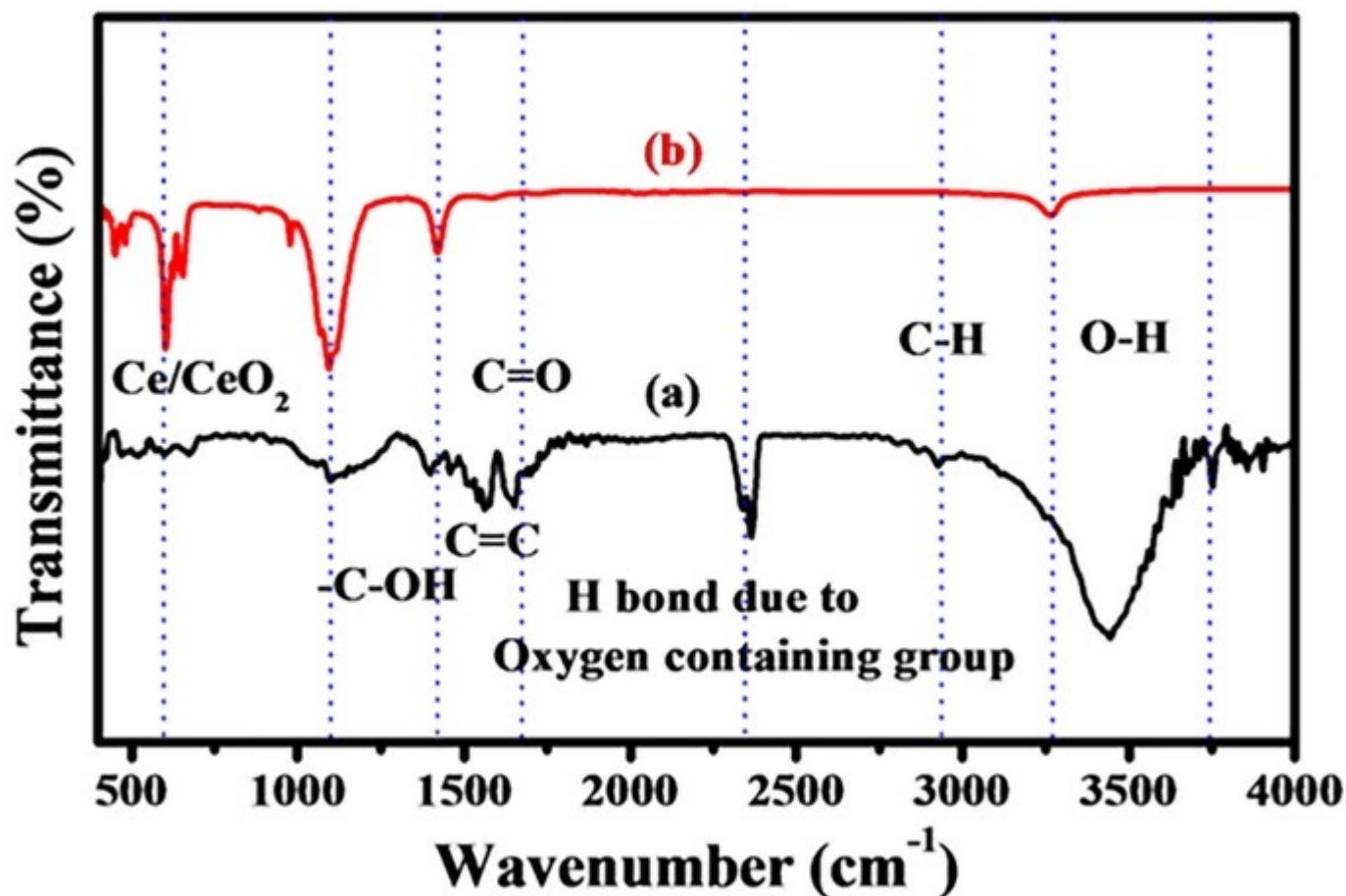
Superimposed Fourier transform infrared (FTIR) spectrum of a rGO and b Ce/CeO_2-rGO nanocomposites, respectively

The N_2-adsorption/desorption isotherms and pore-size distribution of rGO and Ce/CeO_2-rGO hybrid electrocatalytic systems are shown in SI (Fig. S2). Accordingly, in rGO (I) shown in the purple curve presented type-IV isotherm with hysteresis loop, the precise surface area, the average pore size, and the total pore volume of the rGO were analyzed through N_2-adsorption/

desorption isotherms. The hysteresis loop ranges from 0.4 to 0.9 P/P_0. It is well known that the type-IV isotherm is the characteristic isotherm of mesoporous materials [52, 53].

The porosity of the material favors the gas sensitivity and results reflected on quick response towards gas analyte. In this line, the porosity of synthesized composite materials is measured the using Brunauer-Emmett-Teller (BET) technique as shown in SI (Fig. S2). The results indicated that the surface area observed was 41.701 $m^2\,g^{-1}$ v and pore volume 0.065 cc/g with total pore radius of 2.8 nm observed for rGO confirms its porous nature. Typical N_2-adsorption/desorption isotherm of red (II) curve has been shown for Ce/CeO_2-rGO hybrid. Accordingly, the enhancement in surface features after hybrid formation of Ce/CeO_2 with rGO, i.e., of Ce/CeO_2-rGO, was also evaluated and is found to be ~33.297 $m^2\,g^{-1}$ at P/P_0~1; this could be due to the porous nature of Ce/CeO_2-rGO which is probably developed due to the formation of defects on rGO followed by decoration of Ce/CeO_2 at nanodimensions. The isotherm appears to be nearly of type IV in nature which is characteristic of solids containing both micro- and mesopores. The specific BET surface area, total pore volume, and average pore radius were calculated to be 24.780 m^2/g, 1.405 e^{-01} cc/g, and 0.84 nm, respectively, and are in good agreement with hybrids from literature. Literature also reflects that on increasing pore volume and pore radius of that material, the adsorption of gas molecules increases and adsorbs more H_2S gas molecules on the surface of the electrode; ultimately current density has been increased with the rate of sensing [54].

Electrochemical H_2S Sensing on Ce/CeO_2-rGO

Electrochemical studies are with the CH-Electrochemical workstation CHI660E (USA) instrument. The linear sweep voltammetric (LSV) curves of Ce/CeO_2-rGO show potential between −0.55 to 1.1 V vs. SCE in 0.5 M KOH solutions. Once the potential exceeds 0.2 V vs. SCE, a significant decrease in overpotential is observed corresponding to oxidative sensing of H_2S on Ce/CeO_2-rGO with respect to rGO, which could be due to overoxidation of H_2S and the interaction of H_2S molecules at electrified interface, respectively.

Accordingly, Fig. 6a shows the typical linear sweep voltammetry (LSV) of Ce/CeO_2-rGO beyond the potential range of −0.55 V to 1.1 V vs. SCE; the increase in the current originates from the oxidation of the H_2S. Herein, in Fig. 6a curve (iii) a small oxidation peak was observed for the changes in an oxidation state of Ce metal, i.e., from Ce^{+2} to Ce^{+3}. LSV on the

prepared Ce/CeO$_2$–rGO in the presence of H$_2$S was performed to examine electrocatalytic sensitivity towards oxidation of H$_2$S. Practically, in 0.5 M KOH, all H$_2$S species convert to HS$^-$, as it follows the first acid dissociation of H$_2$S molecules and is schematically shown in Scheme 2 and is also reported elsewhere for similar systems [55,56,57,58,59]. Hydrogen sulfide is a weak acid and first dissociates H$_2$S gas (H$_2$S $\leftrightarrow$ H$^+$ + HS$^-$ $\leftrightarrow$ 2H$^+$ + S^{2-}). Also, the electric potential between H$_2$S and O$_2$ is really high, making it extremely favorable for H$_2$S sensing (oxidation reactions); it may be oxidation of (H$_2$S + 2O$_2$ $\rightarrow$ SO$_4^{2-}$ + 2H$^+$) which is catalyzed by metals or metal oxides. Herein, Fig. 6a curve (ii) shows the current density of surface oxide formation signal decreases along with positive shift in potential could be due to adsorption/interaction of H$_2$S molecules and hence hindering further surface oxidation. The typical linear sweep voltammetry has no peaks corresponding to the oxidation and reduction of H$_2$S observed on the bare GC electrode. The LSV performance of Ce/CeO$_2$–rGO in 0.5 M KOH without H$_2$S shows an oxidation signal at ~−0.2 V vs. SCE for surface oxide formation. Furthermore, on Ce/CeO$_2$–rGO in the presence of H$_2$S gas in the same solution, an additional oxidative signal appeared at 0.2 V vs. SCE corresponding to oxidative sensing of H$_2$S. Herein, Table 1 shows a comparative study of electrochemical H$_2$S sensing.

Fig. 6
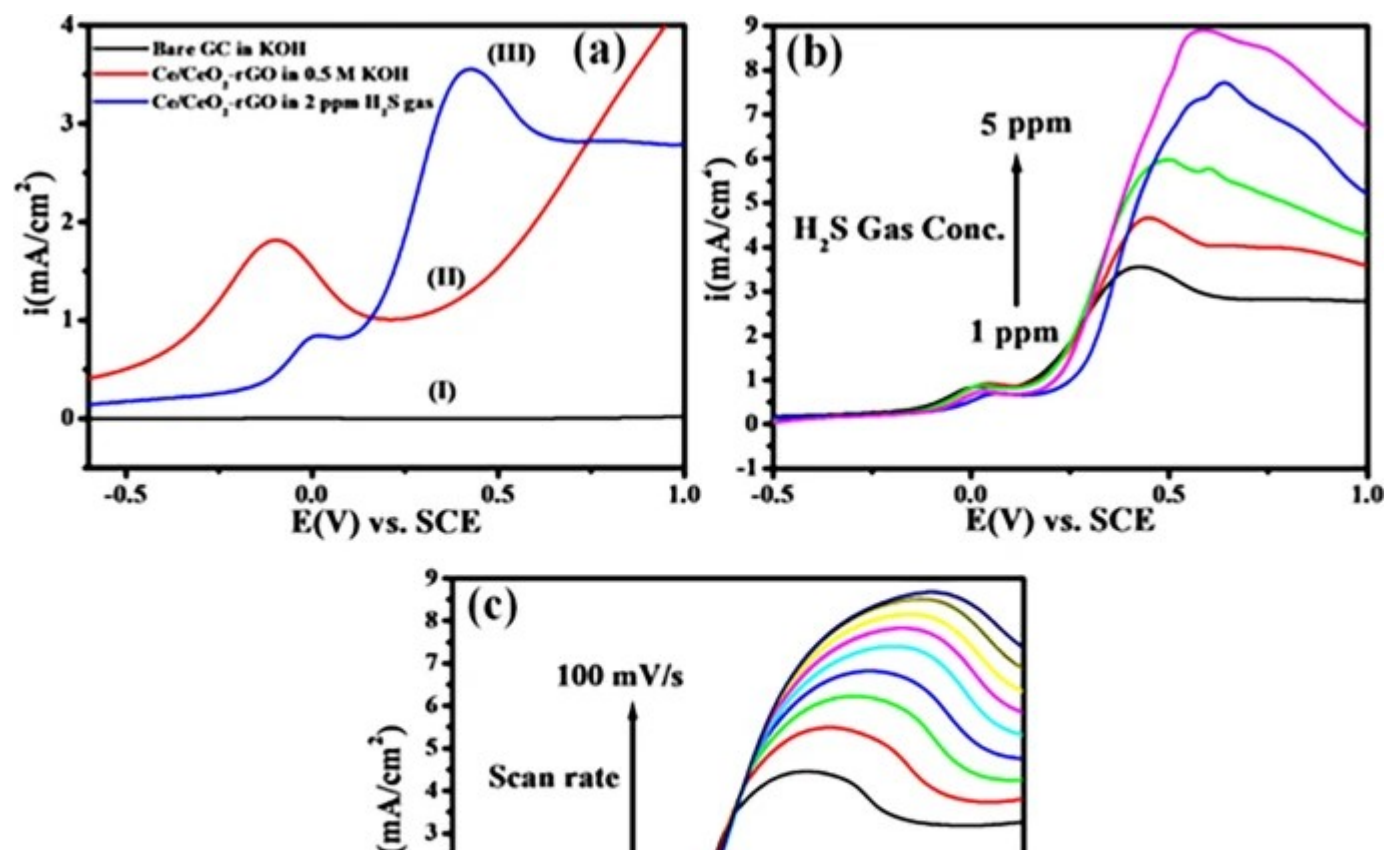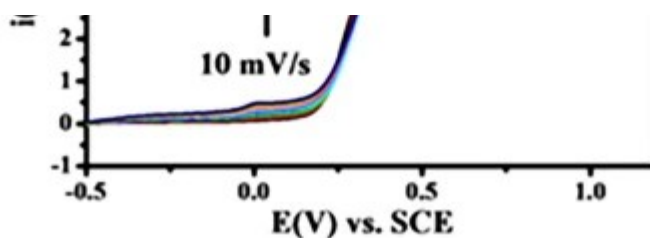
Superimposed LSV curves of a (i) bare GC electrode (black), (ii) Ce/CeO$_2$-rGO (red) in 0.5 M KOH, and (iii) Ce/CeO$_2$-rGO (blue) catalysts in 0.5 M KOH in the presence of 2 ppm H$_2$S gas. The LSV curves of Ce/CeO$_2$-rGO b for different H$_2$S concentrations between 1 and 5 ppm at a scan rate of 50 mV/s, respectively, and c in 0.5 M KOH with 2 ppm H$_2$S gas at different scan rates from 10 to 100 mV/s, respectively, using Pt foil and saturated calomel electrode (SCE) as counter and reference electrodes, respectively

Table 1 Comparative study of electrochemical H$_2$S sensing

To further confirm the electrochemical sensing (oxidation) and H$_2$S concentration, dependent studies have been carried out as shown in Fig. 6b. Accordingly, it represents H$_2$S concentrations. The oxidation current density increases along with a positive shift in potential in the range of 1−5 ppm concentration confirm the H$_2$S sensing at the electrified interface of Ce/CeO$_2$-rGO and with concentration the peak becomes broaden confirms the electrooxidation process is diffusion controlled. Furthermore, the influence of the scan rate on the electrocatalytic oxidation peak potential (E$_{pa}$) and peak current for H$_2$S at 2 ppm concentration on Ce/CeO$_2$-rGO in 0.5 KOH was studied using LSV as shown in Fig. 6c. The current density variation along with a positive shift in potential values was found with an increase in the scan rate from 10 to 100 mV/s and also with a concentration corresponding to diffusion-controlled electron transfer, while here current density increases peak was broadly observed and is in good agreement with the literature [55,56,57,58,59,60,61].

In addition to this, the linearity of concentration vs. current has been determined and it has been shown in Fig. 7 and conforms the current has been increased linearly with the addition of H$_2$S concentration; thus, this methodology is highly applicable for electrochemical sensing of

other toxic gases of H_2S class.

Also, Fig. 7 demonstrated the linearity data at Ce/CeO$_2$–rGO for different H_2S concentrations error bar between 1 and 5 ppm and graphical presentations of linearity data at Ce/CeO$_2$–rGO for different H_2S concentrations between 1 and 5 ppm. The results revealed that the present sensor has good linearity under experimental conditions.

Fig. 7
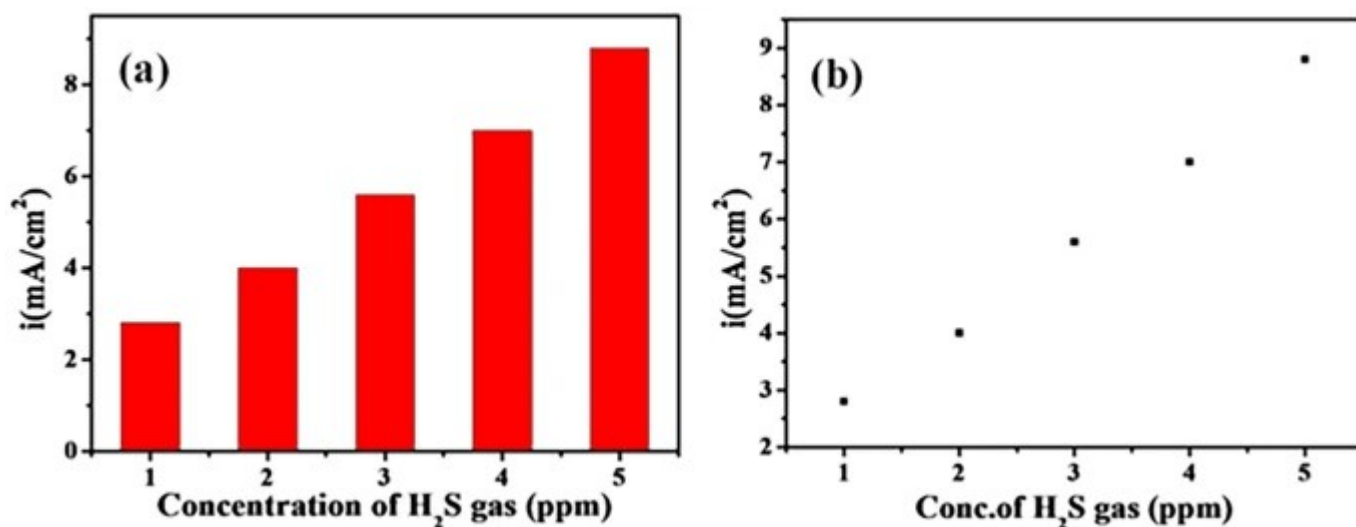
Linearity data at Ce/CeO$_2$–rGO for different H_2S concentrations error bar between 1 and 5 ppm (a and b). The graphical presentations of linearity data at Ce/CeO$_2$–rGO for different H_2S concentrations between 1 and 5 ppm

Furthermore, the applicability of the sensor analyzed by using analytical parameters like LOD and LOQ has been calculated which were found to be 3.24 μM and 10.9 μM, respectively.

The LOD is the lowest analyte concentration at which detection is reasonable. LOQ is the lowest concentration at which the analyte can constantly detect a linear response [60, 61]. Figure 7a indicates typical LSV for different H_2S concentrations between 1 and 5 ppm at a scan rate of 50 mV/s, respectively, and Fig. 7b plot of peak current response vs concentration of H_2S from which we have calculated LOD and LOQ.

LOD and LOQ are calculated using the following equations:

$$\mathrm{LOD} = 3 \;s/m\; \mathrm{and}\; \mathrm{LOQ} = 10 \;s/m$$

where, s is the standard deviation of the intercept and m is the average slope of the regression line.

The present work that calculated LOD and LOQ has been compared with literature and was found to be lower than the report in the literature which is shown in Table 1.

Comparative Electrochemical Studies for H_2S and CO_2 Gases on Ce/CeO_2–rGO

The number of dissolved H_2S molecules in electrolytic solutions results into an increase in adsorption of the gas molecules on Ce/CeO_2–rGO surface producing electro active HS^- ion, and is the further important species representing the qualitative and quantitative sensing of H_2S. There is a superior linear correlation between the peak current and H_2S content in the tested range of 1–5 ppm. In each 20 mL of 0.5 M KOH, electrolytes were taken and dissolved in 1–5 ppm H_2S gas separately and the samples ran on the given potential for LSV. Moreover, this response is also compared with other representative gas, i.e., of CO_2, and it shows no response in the potential range of H_2S oxidation and is shown in Fig. 8. Furthermore, it confirms the selectivity of the sensor in the given range of potential. The results also reveal a new type of low-cost Ce/CeO_2–rGO hybrid sensor for detection of H_2S gas with ultra-high sensitivity and selectivity.

Fig. 8
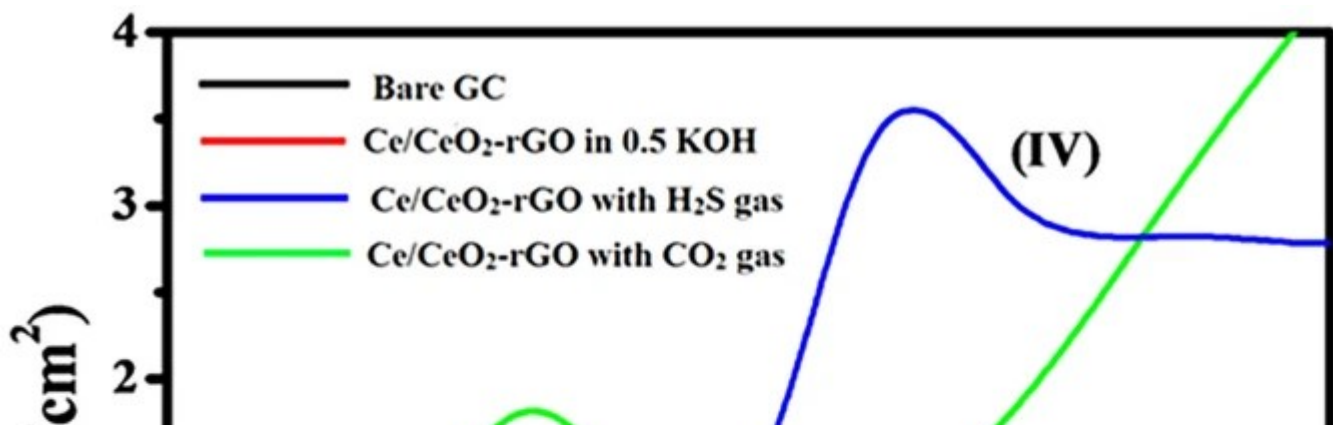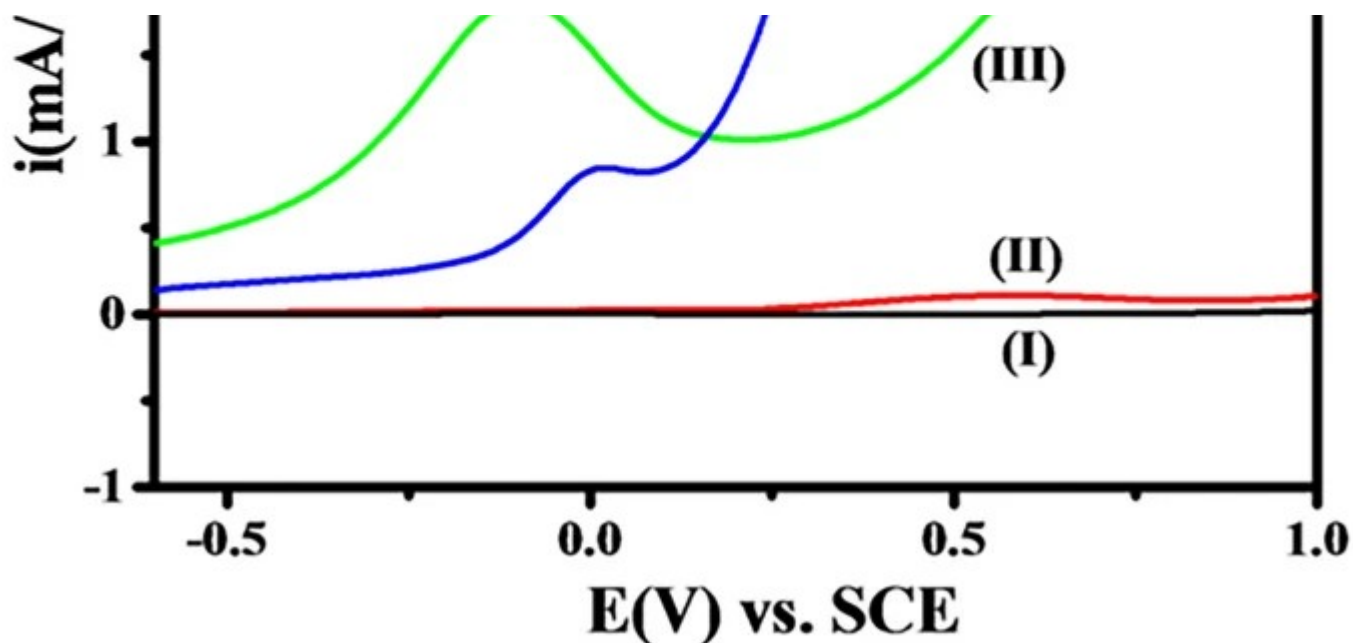
Superimposed linear sweep voltammetry (LSV) for (I) bare GC (black), (II) Ce/CeO$_2$–rGO with CO$_2$ gas (red), (III) Ce/CeO$_2$–rGO (green), and (IV) Ce/CeO$_2$–rGO with 2 ppm H$_2$S gas (blue) in 0.5 M KOH at a scan rate of 50 mV/s, respectively

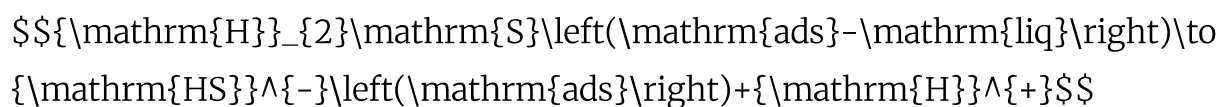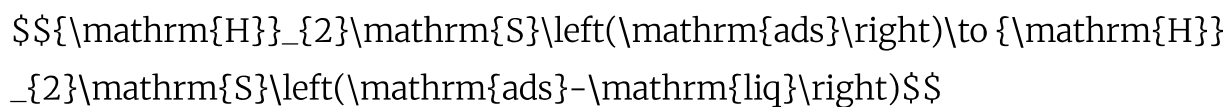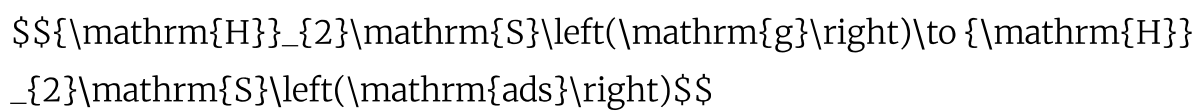## Presumable Mechanistic Path for Electrochemical H$_2$S Sensing

Scheme 3 shows that H$_2$S is first adsorbed on the Ce/CeO$_2$–rGO electrode surface, and then H$_2$S is dissolved in the electrolyte and dissociates further in aqueous electrolytic solutions [62].
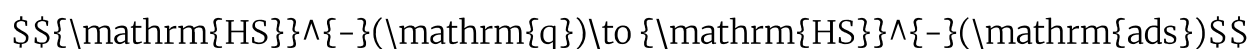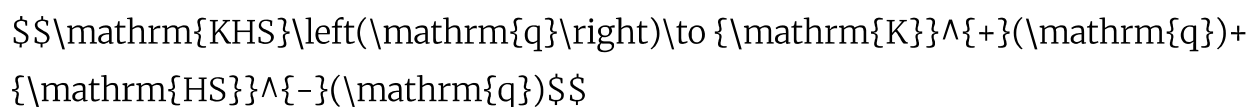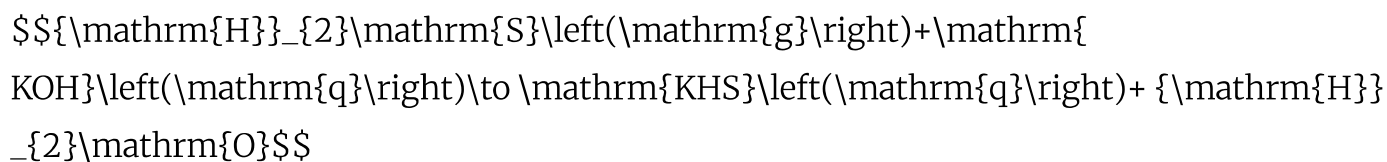
Scheme 3
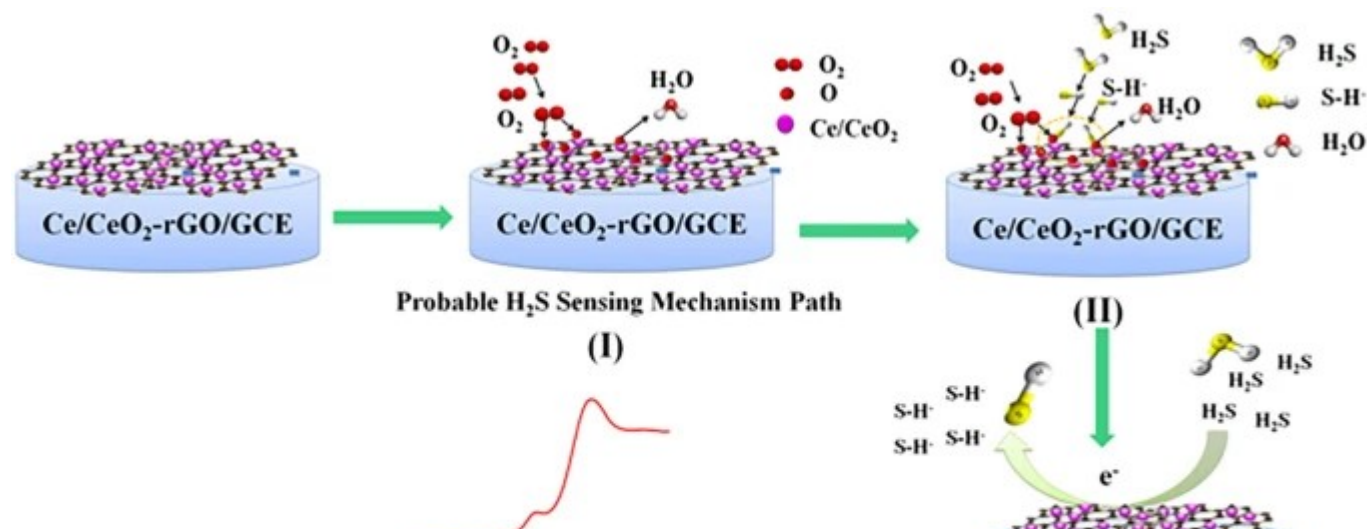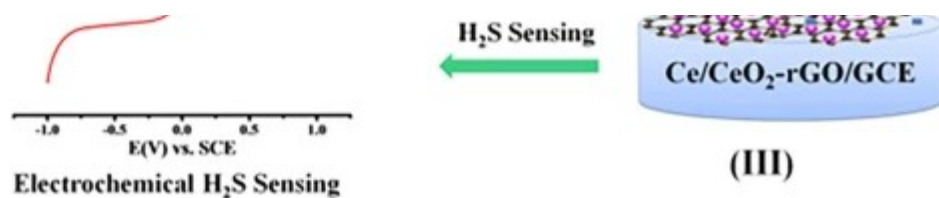
Schematic representation for probable H_2S sensing mechanism involves step (I) Ce/CeO$_2$–rGO and interfacial interactions with species from solution; (II) addition of H_2S gas, whereas, initially dissociation of H_2S to HS^- ions then these HS^- react with oxygen species from solution; and (III) further it gets oxidized at the interface

$${\mathrm{H}}_{2}\mathrm{S}\left(\mathrm{g}\right)\to {\mathrm{H}}_{2}\mathrm{S}\left(\mathrm{ads}\right)$$

$${\mathrm{H}}_{2}\mathrm{S}\left(\mathrm{ads}\right)\to {\mathrm{H}}_{2}\mathrm{S}\left(\mathrm{ads}-\mathrm{liq}\right)$$

$${\mathrm{H}}_{2}\mathrm{S}\left(\mathrm{ads}-\mathrm{liq}\right)\to {\mathrm{HS}}^{-}\left(\mathrm{ads}\right)+{\mathrm{H}}^{+}$$

The probable reaction mechanism is remarkably different when the Ce/CeO$_2$–rGO is in a KOH electrolyte with different pH. When the Ce/CeO$_2$–rGO is exposed to high pH, i.e., pH > 7, a huge number of active sites are available; hence, chemisorption dominates and this is the beginning of H_2S adsorption [58, 59].

$${\mathrm{H}}_{2}\mathrm{S}\left(\mathrm{g}\right)+\mathrm{KOH}\left(\mathrm{q}\right)\to \mathrm{KHS}\left(\mathrm{q}\right)+ {\mathrm{H}}_{2}\mathrm{O}$$

$$\mathrm{KHS}\left(\mathrm{q}\right)\to {\mathrm{K}}^{+}(\mathrm{q})+ {\mathrm{HS}}^{-}(\mathrm{q})$$

$${\mathrm{HS}}^{-}(\mathrm{q})\to {\mathrm{HS}}^{-}(\mathrm{ads})$$

However, Ce/CeO$_2$–based nanomaterials have been commonly used in numerous fields

including catalysis, adsorption, sensing, H_2 production, photo and electrocatalysis, semiconductor devices, fuel cells, and biomedical devices. Cerium (Ce) Ce^{3+}, 0.1143 nm; Ce^{4+}, 0.097 nm, favors extensive solubility with the ceria lattice and it increases the trivalent state of Ce, which may further enhance the activity of ceria. Herein, the electrochemical H_2S sensing studies on Ce/CeO_2 show a strong oxidizing agent in association with oxygen atoms. Cerium oxide (CeO_2) is one of the important transition metal oxides which are acting as n-type semiconductors. It exists as both cerous Ce^{3+}, trivalent state, and ceric Ce^{4+}, a tetravalent state in the form of compounds, as an electrochemical H_2S sensing performance of Ce/CeO_2-rGO hybrids is better as compared with reports from the literature. For example, Qing et al. reported a mono-ethanolamine hydroxyl-functionalized ionic liquid–enabled electrochemical sensor for the detection of H_2S and our report reflects better oxidation performance toward H_2S sensing at a very lower detection (ppm) limit [63, 64]. The main exclusive characters of CeO_2 involve a band gap of 3−3.6 eV and the ability to turn their oxidation state in a gas environment and an easy path for electron transfer through rGO. The novelty of this work includes the synthesis of Ce/CeO-rGO nanomaterial; herein, the Ce/CeO_2 nanoparticles were decorated on rGO by chemical synthesis and used for electrochemical study on H_2S gas sensing approach for the first time. The beauty of choice for Ce is having a tuneable oxidation state, i.e., Ce^{3+}/Ce^{4+} coupled and combined with a potential candidate, i.e., rGO for H_2S determination.

Conclusion

The Ce/CeO_2-rGO based electrode system exhibited a highly sensitive and selective response at low potential towards oxidative electrochemical H_2S sensing. There is a linear relationship between oxidative current density and the H_2S content in the tested ultra-low range, i.e., of 1−5 ppm. The cross-sensitivity of the proposed sensor was tested towards CO_2 along with H_2S in the same potential range and found there are no oxidation peaks observed. Furthermore, for the applicability of sensor, the analytical parameters like LOD and LOQ have been calculated and were found to be 3.24 µM and 10.9 µM, respectively. Our findings on Ce/CeO_2-rGO nanocomposites for the electrochemical detection of H_2S open up a new and efficient method for H_2S other class of gas sensing. The H_2S sensing response has been examined in basic pH and suitable oxidative pathways have been proposed for the oxidation process under alkaline

conditions.

Availability of Data and Materials

No, all of the materials are owned by the authors and/or no permissions are required.

References

1. E.A.Q. Mooyaart, E.L.G. Gelderman, M.W. Nijsten, R. Vos, J.M. Hirner, D.W. Lange, H.D.G. Leuvenink, W.M. Bergh, Outcome after hydrogen sulphide intoxication. Resuscitation. 103, 1–6 (2016). https://doi.org/10.1016/j.resuscitation.2016.03.012

   Article PubMed Google Scholar

2. J.R. Hall, M.H. Schoenfisch, Direct electrochemical sensing of hydrogen sulfide without sulfur poisoning. Anal. Chem. 90, 5194–5200 (2018). https://doi.org/10.1021/acs.analchem.7b05421

   Article CAS PubMed PubMed Central Google Scholar

3. J. Jiang, A. Chan, S. Ali, A. Saha, K.J. Haushalter, W.L.M. Lam, M. Glasheen, J. Parker, M. Brenner, S.B. Mahon, H.H. Patel, R. Ambasudhan, S.A. Lipton, R.B. Pilz, G.R. Bos, Hydrogen sulfide-mechanisms of toxicity and development of an antidote. Sci. Rep. 6, 20831 (2016). https://doi.org/10.1038/srep20831

4. S.L.M. Rubright, L.L. Pearce, J. Peterson, Environmental toxicology of hydrogen sulphide. Nitric Oxide. 71, 1–13 (2017). https://doi.org/10.1016/j.niox.2017.09.011

   Article CAS Google Scholar

5. J. Sun, L. Li, G. Zhou, X. Wang, L. Zhang, Y. Liu, J. Yang, X. Lu, F. Jiang, Biological sulfur reduction to generate H2S as a reducing agent to achieve simultaneous catalytic removal of SO2 and NO and sulfur recovery from flue gas. Environ. Sci. Technol. 52, 4754−4762 (2018). https://doi.org/10.1021/acs.est.7b06551

Article CAS PubMed Google Scholar

6. W. Rumbeiha, E. Whitley, P. Anantharam, D.S. Kim, A. Kanthasamy, Acute hydrogen sulphide-induced neuropathology and neurological sequelae: challenges for translational neuroprotective research. Ann. N.Y. Acad. Sci. 1378, 5-16 (2016). https://doi.org/10.1111/nyas.13148

7. B. Jelen, D. Giovannelli, P.G. Falkowski, C. Vetriani, Elemental sulfur reduction in the deep-sea vent thermophile. Environ. Microbiol. 20, 2301−2316 (2018). https://doi.org/10.1111/1462-2920.14280

Article CAS PubMed Google Scholar

8. H. brahima, A. Serag, M.A. Farag, Emerging analytical tools for the detection of the third gasotransmitter H2S a comprehensive review. J. Adv. Res. 27, 137-153 (2021). https://doi.org/10.1016/j.jare.2020.05.018

9. J. Furne, A. Saeed, M.D. Levitt, Whole tissue hydrogen sulfide concentrations are orders of magnitude lower than presently accepted values. Am. J. Physiol.: Regul, Integr. Comp. Physiol. 295, RR1479−R1485 (2008). https://doi.org/10.1152/ajpregu.90566.2008

10. M.D. Levitt, M.S. Abdel-Rehim, J. Furne, Free and acid-labile hydrogen sulfide concentrations in mouse tissues: anomalously high free hydrogen sulfide in aortic tissue. Antioxid. Redox Signaling. 15, 373–378 (2011). https://doi.org/10.1089/ars.2010.3525

Article   CAS   Google Scholar

11. X. Shen, C.B. Pattillo, S. Pardue, S.C. Bir, R. Wang, C.G. Kevil, Measurement of plasma hydrogen sulfide in vivo and in vitro. Free Radicals Biol. Med. 50, 1021–1031 (2011). https://doi.org/10.1016/j.freeradbiomed.2011.01.025

Article   CAS   Google Scholar

12. E.A. Wintner, T.L. Deckwerth, W. Langston, A. Bengtsson, D. Leviten, P. Hill, M.A. Insko, R. Dumpit, E. VandenEkart, C.F. Toombs, C. Szabo, A monobromobimane-based assay to measure the pharmacokinetic profile of reactive sulphide species in blood. Br. J. Pharmacol. 160, 941–957 (2010). https://doi.org/10.1111/j.1476-5381.2010.00704.x

Article   CAS   PubMed   PubMed Central   Google Scholar

13. M. Nishida, T. Sawa, N. Kitajima, K. Ono, H. Inoue, H. Ihara, H. Motohashi, M. Yamamoto, M. Suematsu, H. Kurose, A. van der Vliet, B.A. Freeman, T. Shibata, K. Uchida, Y. Kumagai, T. Akaike, Hydrogen sulfide anion regulates redox signaling via electrophile sulfhydration. Nat. Chem. Biol. 8, 714–724 (2012). https://doi.org/10.1038/nchembio.1018

Article   CAS   PubMed   PubMed Central   Google Scholar

14. X. Shen, G. K. Kolluru, S. Yuan and C. G. Kevil, Measurement of H2S In Vivo and In Vitro by the Monobromobimane Method. Methods Enzymol, ed. C. Enrique, P. Lester, Roary. Academic Press. 554, 31–45 (2015). https://doi.org/10.1016/bs.mie.2014.11.039

15. X. Hu, B. Mutus, Electrochemical detection of sulphide. Rev. Anal. Chem. 32, 247–256 (2013). https://doi.org/10.1515/revac-2013-0008

Article　CAS　Google Scholar

16. D.W. Kraus, J.E. Doeller, X. Zhang, J. Wang, X. Zhang, J. Huangxian, Electrochemical hydrogen sulfide biosensors. Academic Press, San Diego. 213-229 (2008). https://doi.org/10.1039/C5AN02208H

17. S.K. Pandey, K.H. Kim, K.T. Tang, A review of sensor-based methods for monitoring hydrogen sulphide. TrAC Trends Anal. Chem. 32, 87–99 (2012). https://doi.org/10.1016/j.trac.2011.08.008

Article　CAS　Google Scholar

18. N.S. Lawrence, J. Davis, R.G. Compton, Analytical strategies for the detection of sulfide: a review. Talanta. 52, 771–784 (2000). https://doi.org/10.1016/S0039-9140(00)00421-5

Article　CAS　PubMed　Google Scholar

19. A. Afkhami, L. Khalafi, Indirect determination of sulfide by cold vapor atomic absorption spectrometry. Microchim. Acta. 150, 43–46 (2005). https://doi.org/10.1007/s00604-005-0344-5

Article　CAS　Google Scholar

20. S. Shah, Md.A. Aziz, M. Oyama, A.R.F. Albatar, Controlled-potential-based electrochemical sulfide sensors: a review. Chem. Rec. 21, 204–238 (2021). https://doi.org/10.1002/tcr.202000115

Article　CAS　PubMed　Google Scholar

21. H. Peng, Strategies in developing fluorescent probes for live cell imaging and quantitation of hydrogen sulfide. JSM Biotechnol Biomed Eng. 1, 1018, 1-3 (2013).

https://doi.org/10.47739/2333-7117/1018

22. Z. Pawlak, A. S. Pawlak, Modification of iodometric determination of total and reactive sulfide in environmental sample. Talanta 48(2):347–353 (1999)

23. A. Aziz, S.S. Shah, A. Kashem, Preparation and utilization of jute-derived carbon: a short review. Chem. Rec. 20, 1074−1098 (2020). https://doi.org/10.1002/tcr.202000071

Article   CAS   PubMed   Google Scholar

24. A.J.S. Ahammad, N. Odhikari, S.S. Shah, M.M. Hasan, T. Islam, P.R. Pal, M.A. Ahmed Qasem, M.A. Aziz, Porous tal palm carbon nanosheets: preparation, characterization and application for the simultaneous determination of dopamine and uric acid. Nanoscale Adv.1, 613-626 (2019). https://doi.org/10.1039/C8NA00090E

25. B.B. Mulik, A.V. Munde, R.P. Dighole, B.R. Sathe, Electrochemical determination of semicarbazide on cobalt oxide nanoparticles: implication towards environmental monitoring. J Ind Eng Chem. 93, 259−266 (2021). https://doi.org/10.1016/j.jiec.2020.10.002

Article   CAS   Google Scholar

26. S.M. Mali, S.S. Narwade, Y.H. Navale, S.B. Tayade, R.V. Digraskar, V.B. Patil, A.S. Kumbhar, B.R. Sathe, Heterostructural CuO−ZnO nanocomposites: a highly selective chemical and electrochemical NO2 sensor. ACS Omega. 4, 20129−20141 (2019). https://doi.org/10.1021/acsomega.9b01382

27. S.S. Shah, M.A. Alfasane, I.A. Bakare, M.A. Aziz, Z.H. Yamani, Polyaniline and heteroatoms−enriched carbon derived from Pithophora polymorpha composite for high performance supercapacitor. J. Energy Storage. 30, 101562 (2020). https://

doi.org/10.1016/j.est.2020.101562

28. H. Shang, H. Xu, L. Jin, C. Wang, C. Chen, T. Song, Y. Du, 3D ZnIn2S4 nanosheets decorated ZnCdS dodecahedral cages as multifunctional signal amplification matrix combined with electroactive/photoactive materials for dual mode electrochemical - photoelectrochemical detection of bovine haemoglobin. Biosens. Bioelectron. 159, 112202 (2020). https://doi.org/10.1016/j.bios.2020.112202

29. Y. Zhao, Y. Yang, L. Cui, F. Zheng, Q. Song, Electroactive Au@Ag nanoparticles driven electrochemical sensor for endogenous H2S detection. Biosens. Bioelectron. 117, 53−59 (2018). https://doi.org/10.1016/j.bios.2018.05.047

Article   CAS   PubMed   Google Scholar

30. M. Asif, A. Aziz, Z. Wang, G. Ashraf, J. Wang, H. Luo, X. Chen, F. Xiao, H. Liu, Hierarchical CNTs@CuMn layered double hydroxide nanohybrid with enhanced electrochemical performance in H2S detection from live cells. Anal. Chem. 91, 3912−3920 (2019). https://doi.org/10.1021/acs.analchem.8b04685

Article   CAS   PubMed   Google Scholar

31. A. Shanmugasundaram, N.D. Chinh, Y.J. Jeong, T.F. Hou, D.S. Kim, D. Kim, Y.B. Kim, D.W. Lee, Hierarchical nanohybrids of B- and N-codoped graphene/mesoporous NiO nanodisks: an exciting new material for selective sensing of H2S at near ambient temperature. J. Mater. Chem. A. 7, 9263−9278 (2019). https://doi.org/10.1039/C9TA00755E

Article   CAS   Google Scholar

32. M.A. Haija, A.F.S. Abu-Hani, N. Hamdan, S. Stephen, A.I. Ayesh, Characterization of H2S gas sensor based on CuFe2O4 nanoparticles. J. Alloys Compd. 690, 461−468 (2017). https://doi.org/10.1016/j.jallcom.2016.08.174

Article   CAS   Google Scholar

33. H. Shang, H. Xu, Q. Liu, Y. Du, PdCu alloy nanosheets-constructed 3D flowers: new highly sensitive materials for H2S detection. Sens. Actuators, B. 289, 260-268 (2019). https://doi.org/10.1016/j.snb.2019.03.101

34. M. Asad, M.H. Sheikhi, M. Pourfath, M. Moradi, High sensitive and selective flexible H2S gas sensors based on Cu nanoparticle decorated SWCNTs. Sens. Actuators B. 210, 1−8 (2015). https://doi.org/10.1016/j.snb.2014.12.086

Article   CAS   Google Scholar

35. P. Balasubramanian, S.B. He, H.H. Deng, H.P. Peng, W. Chen, Defects engineered 2D ultrathin cobalt hydroxide nanosheets as highly efficient electrocatalyst for non-enzymatic electrochemical sensing of glucose and l-cysteine. Sens. Actuators, B. 320, 128374 (2020). https://doi.org/10.1016/j.snb.2020.128374

36. N. Ahmad, A.S. Al-Fatesh, R. Wahab, M. Alam, A.H. Fakeeha, Synthesis of silver nanoparticles decorated on reduced graphene oxide nanosheets and their electrochemical sensing towards hazardous 4-nitrophenol. J. Mater. Sci.: Mater. Electron.31, 11927-11937 (2020). https://doi.org/10.1007/s10854-020-03747-3

37. M.D. Brown, J.R. Hall, M.H. Schoenfisch, A direct and selective electrochemical hydrogen sulfide sensor. AnalyticaChimica Acta. 1045, 67-76 (2019). https://doi.org/10.1016/j.aca.2018.08.054

38. D. Filotasac, I.Z. Batai, G. Pozsgaia, L. Nagya, E. Pintéra, G. Nagya, Highly sensitive potentiometric measuring method for measurement of free H2S in physiologic samples. Sens. Actuators B Chem. 243, 326−331 (2017). https://doi.org/10.1016/j.snb.2016.11.102

Article CAS Google Scholar

39. Agency for Toxic Substances and Disease Registry, Toxicological profile for hydrogen sulfide, U. S. Department of Health and Human Services, Public Health and services. Atlanta, Georgia, 137 (2006). https://www.atsdr.cdc.gov/toxprofiles/tp114.pdf

40. B.R. Sathe, M.S. Risbud, S. Patil, K.S. Ajayakumar, R.C. Naik, I.S. Mulla, V. K. Pillai, Highly sensitive nanostructured platinum electrocatalysts for CO oxidation: Implications for CO sensing and fuel cell performance. Sens. Actuators A: Phys 138(2), 376−383 (2007). https://doi.org/10.1016/j.sna.2007.05.013

41. N.S. Lawrence, L. Jiang, T.G.J. Jones, R.G. Compton, A thin-layer amperometric sensor for hydrogen sulfide: the use of microelectrodes to achieve a membrane-independent response for clark-type. Sensors. Anal. Chem. 75, 2499 (2003). https://doi.org/10.1021/ac0206465

Article CAS PubMed Google Scholar

42. E. Zdrachek, E. Bakker, Potentiometric Sensing. Anal. Chem. 91, 2-26 (2019). https://doi.org/10.1021/acs.analchem.8b04681

43. B. Peng , J. Cui, Y. Wang, J. Liu, H. Zheng, L. Jin, X. Zhang, Y. Zhang, Y. Wu, CeO2-x/C/rGO nanocomposites derived from Ce-MOF and graphene oxide as a robust platform for highly sensitive uric acid detection. Nanoscale.10, 1939-1945 (2018). https://doi.org/10.1039/C7NR08858B

44. Q. Diao, Y. Yin, W. Jia, X. Xu, Y. Ding, X. Zhang, J. Cao, K. Yang, Highly sensitive ethanol sensor based on Ce-doped WO3 with raspberry-like architecture. Mater. Res. Express.7, 115012 (2020). https://iopscience.iop.org/article/doi.org/10.1088/2053-1591/abcabf

45. P.P. Chavan, V.S. Sapner, A. V Munde, S. M Mali, B.R. Sathe, Synthesis of metal–free nanoporous carbon with few–layer graphene electrocatalyst for electrochemical NO2– oxidation. ChemistrySelect.6, 9847–9852 (2021). https://doi.org/10.1002/slct.202102625

46. S.S. Narwade, S.M. Mali, A.K. Tapre, B.R. Sathe, Enhanced electrocatalytic H_2S splitting on a multiwalled carbon nanotubes-graphene oxide nanocomposite. NJC. 45, 20266–20271 (2021). https://doi.org/10.1039/D1NJ00432H

47. S.S. Narwade, S.M. Mali, R.V. Digraskar, V.S. Sapner, B.R. Sathe, Ni/NiO@rGO as an efficient bifunctional electrocatalyst for enhanced overall water splitting reactions. Int. J. Hydrog. Energy. 44, 27001–27009 (2019).https://doi.org/10.1016/j.ijhydene.2019.08.147

48. V.S. Sapner, P.P. Chavan, R.V. Digraskar, S.S. Narwade, B.B. Mulik, S.M. Mali, B.R. Sathe, Tyramine functionalized graphene: metal–free electrochemical non–enzymatic biosensing of hydrogen peroxide. Chem Electro Chem. 5, 3191–3197 (2019). https://doi.org/10.1002/celc.201801083

49. B.B. Mulik, B.D. Bankar, A.V. Munde, A.V. Biradar, T. Asefa and B.R. Sathe, Facile synthesis and characterization of γ–Al 2 O 3 loaded on reduced graphene oxide for electrochemical reduction of CO 2, Sustain. Energy Fuels. 6, 5308–5315 (2022). https://doi.org/10.1039/D2SE00953F

50. S. Sagadevan, M.R. Johan, J. AnitaLett, Fabrication of reduced graphene oxide/CeO_2 nanocomposite for enhanced electrochemical performance. Appl. Phys. A. 125, 315 (2019).https://doi.org/10.1007/s00339-019-2625-6

51. S. Wang, F. Gao, Y. Zhao, N. Liu, T. Tan, X. Wang, Two–dimensional CeO2/RGO composite–modified separator for lithium/sulfur batteries. Nanoscale Res. Lett. 377, 1−9 (2018). https://doi.org/10.1186/s11671-018-2798-5

Article   CAS   Google Scholar

52. A.V. Munde, B.B. Mulik, P.P. Chavan, V.S. Sapner, S.S. Narwade, S.M. Mali, B.R. Sathe, Electrocatalytic ethanol oxidation on cobalt−bismuth nanoparticle-decorated reduced graphene oxide (Co−Bi@rGO): reaction pathway investigation toward direct ethanol fuel cells. J. Phys. Chem. C. 4, 2345-2356 (2021). https://doi.org/10.1039/C7RA11676D

53. R. Vinoth, P. Karthik, C. Muthamizhchelvan, B. Neppolian, M. Ashokkumar, Carrier separation and charge transport characteristics of reduced graphene oxide supported visible-light active photocatalysts. Phys. Chem. Chem. Phys. 18, 5179−5191 (2016). https://doi.org/10.1039/C5CP08041J

Article   CAS   PubMed   Google Scholar

54. B.B. Mulik, B.D. Bankar, A.V. Munde, A.V. Biradar, B.R. Sathe, Bismuth-oxide-decorated graphene oxide hybrids for catalytic and electrocatalytic reduction of CO2Chem. Eur. J. 26, 8801−8809 (2020). https://doi.org/10.1002/chem.202001589

Article   CAS   Google Scholar

55. E.A. Khudaish, A.T. Al-Hinai, The catalytic activity of vanadium pentoxide film modified electrode on the electrochemical oxidation of hydrogen sulfide in alkaline solutions. J. Electro Chem. 587, 108−114 (2006). https://doi.org/10.1016/j.jelechem.2005.10.023

Article   CAS   Google Scholar

56. H. Selvaraj, K. Chandrasekarana, R. Gopalkrishnan, Recovery of solid sulfur from hydrogen sulfide gas by an electrochemical membrane cell. RSC Adv. 6, 3735−3741 (2016). https://doi.org/10.1039/C5RA19116E

Article   CAS   Google Scholar

57. L. Wang, P. Lu, C. Liu, L. Wang, Electro-oxidation of sulfide on Ti/RuO2 electrode in an aqueous alkaline solution. Int. J. Electrochem. Sci. 10, 8374 (2015). https://www.semanticscholar.org/paper/Electro-oxidation-of-Sulfide-on-Ti-RuO2-Electrode-Wang-Lu/579c6002f699f3c6ddee95b3ec47387851a7ee46

58. Y. Triana, M. Tomisaki, Y. Einaga. Oxidation reaction of dissolved hydrogen sulfide using boron doped diamond. J. Electroanal. Chem. 873, 114411 (2020). https://doi.org/10.1016/j.jelechem.2020.114411

59. X. Liu, L. He, P. Li, X. Li, P. Zhang, A direct electrochemical H2S sensor based on Ti3C2Tx MXene. ChemElectroChem. 8, 3658-3665 (2021). https://doi.org/10.1002/celc.202100964

60. B.B. Mulik, S.T. Dhumal, V.S. Sapner, N.N.M.A. Rehman, P.P. Dixit, B.R. Sathe, Graphene oxide-based electrochemical activation of ethionamide towards enhanced biological activity. RSC Adv. 9, 35463-35472 (2019). https://doi.org/10.1039/C9RA06681K

61. T.J. Ehirim, O.C. Ozoemena, P.V. Mwonga, A.B. Haruna, T.P. Mofokeng, K.D. Wael, K.I. Ozoemena, Onion-like carbons provide a favorable electrocatalytic platform for the sensitive detection of tramadol drug, ACS Omega. 7, 47892-47905 (2022). https://doi.org/10.1021/acsomega.2c05722

62. X. Zhang, Y. Tang, S. Qu, J. Da, Z. Hao, H2S-selective catalytic oxidation: catalysts and processes. ACS Catal. 5, 1053−1067 (2015). https://doi.org/10.1021/cs501476p

Article CAS Google Scholar

63. Q. Huang, W. Li, T. Wu, X. Ma, K. Jiang, X. Jin. Monoethanolamine-enabled electrochemical detection of H2S in a hydroxyl-functionalized ionic liquid. ElectrochemComm. 88, 93-96 (2018). https://doi.org/10.1016/j.elecom.2017.12.024

64. K. Mukherjee, A.P.S. Gaur, S.B. Majumder, Investigations on irreversible- and reversible-type gas sensing for ZnO and Mg0.5Zn0.5Fe2O4 chemi-resistive sensors. J. Phys. D: Appl. Phys. 45, 505306 (2012). https://doi.org/10.1088/0022-3727/45/50/505306

Acknowledgements

Funding

Author information

Authors and Affiliations

Department of Chemistry, Dr. Babasaheb Ambedkar, Marathwada University, Aurangabad, 431004, India

Shivsharan M. Mali, Shankar S. Narwade, Balaji B. Mulik, Vijay S. Sapner, Shubham J. Annadate & Bhaskar R. Sathe

University Department of Basic and Applied Sciences, MGM University, Aurangabad, 431005, India

Balaji B. Mulik

Department of Nanotechnology, Dr. Babasaheb Ambedkar, Marathwada University, Aurangabad, 431004, India

Bhaskar R. Sathe

Contributions

Shivsharan M. Mali and Shankar S. Narwade wrote the manuscript. Balaji B. Mulik and Vijay S. Sapner supported for characterization, analyzed, and helped electrochemical measurements. Shubham J. Annadate helped synthesize sensor materials. Dr Bhaskar Sathe gave the idea, guided all the projects, and reviewed the manuscript.

Corresponding author

Correspondence to Bhaskar R. Sathe.

Ethics declarations

Ethical Approval

Not applicable

Competing Interests

The authors declare no competing interests.

Additional information

Publisher's Note

Springer Nature remains neutral with regard to jurisdictional claims in published maps and institutional affiliations.

Supplementary Information

Below is the link to the electronic supplementary material.

Supplementary file1 (DOCX 278 KB)

Rights and permissions

Reprints and permissions

About this article

Cite this article

Share this article

Anyone you share the following link with will be able to read this content:

Get shareable link

Keywords

[Ce/CeO$_2$-rGO hybrid nanoelectrodes](#)   [Environmental monitoring](#)   [H$_2$S seneor](#)

[Sensitivity and selectivity](#)   [Electrochemical gas sensor](#)